CMI

www.nature.com/cmi

ARTICLE

Check for updates

Integrated NLRP3, AIM2, NLRC4, Pyrin inflammasome activation and assembly drive PANoptosis

SuHyeon Oh[1,3], Jihye Lee[1,3], Jueun Oh[1], Gyoengju Yu[1], Haesun Ryu[2], Daesik Kim[2] and SangJoon Lee[1]✉

Inflammasomes are important sentinels of innate immune defense; they sense pathogens and induce the cell death of infected cells, playing key roles in inflammation, development, and cancer. Several inflammasome sensors detect and respond to specific pathogen- and damage-associated molecular patterns (PAMPs and DAMPs, respectively) by forming a multiprotein complex with the adapters ASC and caspase-1. During disease, cells are exposed to several PAMPs and DAMPs, leading to the concerted activation of multiple inflammasomes. However, the molecular mechanisms that integrate multiple inflammasome sensors to facilitate optimal host defense remain unknown. Here, we discovered that simultaneous inflammasome activation by multiple ligands triggered multiple types of programmed inflammatory cell death, and these effects could not be mimicked by treatment with a pure ligand of any single inflammasome. Furthermore, NLRP3, AIM2, NLRC4, and Pyrin were determined to be members of a large multiprotein complex, along with ASC, caspase-1, caspase-8, and RIPK3, and this complex drove PANoptosis. Furthermore, this multiprotein complex was released into the extracellular space and retained as multiple inflammasomes. Multiple extracellular inflammasome particles could induce inflammation after their engulfment by neighboring macrophages. Collectively, our findings define a previously unknown regulatory connection and molecular interaction between inflammasome sensors, which drives the assembly of a multiprotein complex that includes multiple inflammasome sensors and cell death regulators. The discovery of critical interactions among NLRP3, AIM2, NLRC4, and Pyrin represents a new paradigm in understanding the functions of these molecules in innate immunity and inflammasome biology as well as identifying new therapeutic targets for NLRP3-, AIM2-, NLRC4- and Pyrin-mediated diseases.

Keywords: Multiple Inflammasome; Inflammatory Cell Death; PANoptosis; Excellular ASC; PANoptosome

Cellular & Molecular Immunology; https://doi.org/10.1038/s41423-023-01107-9

INTRODUCTION

Inflammasomes are important sentinels of innate immune defense that facilitate host protection against infection [1]. After exposure to pathogen- and damage-associated molecular patterns (PAMPs and DAMPs, respectively), inflammasome sensors form a multiprotein complex that activates caspase-1, leading to the cleavage of its downstream substrates, inflammatory signaling, and inflammatory cell death. Well-established inflammasome sensors and their cognate triggers that have been characterized to date include NLRP1 (*Bacillus anthracis* lethal factor [2], N-terminal proteasomal degradation [3, 4], enteroviral 3C protease activity [5], and long dsRNA [6]), NLRP3 (ATP, pore-forming toxins, and uric acid crystals), NLRC4 (bacterial flagellin and type III secretion system components), AIM2 (dsDNA), and pyrin (inactivation of Rho-GTPase activity) [1]. While individual inflammasome sensors detect and respond to specific PAMPs and DAMPs, emerging evidence suggests that multiple inflammasome sensors can be activated in response to disease, particularly live-pathogen infections, owing to the presence of multiple PAMPs and DAMPs. For instance, the AIM2 and NLRP3 inflammasomes are both activated during *Aspergillus* infection [7]; NLRC4 and NLRP3 mediate the clearance of *Salmonella* infection [8, 9]; NLRP3 and AIM2 both contribute to inflammasome-dependent cytokine release in response to *Plasmodium* infection [10]; and AIM2, Pyrin, and ZBP1 form multiple inflammasomes in single cells to drive inflammatory cell death and host defense in response to herpes simplex virus 1 (HSV1) or *Francisella novicida* infection [11].

Inflammasome activation is associated with gasdermin D (GSDMD)-mediated pyroptosis. However, several critical functions have been observed for single inflammasome sensors beyond their canonically described roles in inflammasome formation and pyroptosis, and these functions cannot be explained by our current understanding of inflammasome biology; these functions include the ability of multiple inflammasome sensors to recruit both pyroptotic caspase-1 and apoptotic caspase-8 to the same cell death complex and induce multiple programmed cell death (PCD) pathways [7, 11]. Multiple pathogen-derived PAMPs and DAMPs can also lead to extensive crosstalk between PCD pathways and promote multiple forms of PCD, including pyroptosis, apoptosis, and necroptosis [11–20]. However, the specific PAMPs and DAMPs that trigger large multiprotein

[1]Department of Biological Science, Ulsan National Institute of Science and Technology (UNIST), Ulsan, Republic of Korea. [2]Department of Precision Medicine, Sungkyunkwan University School of Medicine, Suwon, Republic of Korea. [3]These authors contributed equally: SuHyeon Oh, Jihye Lee. ✉email: sangjoon.lee@unist.ac.kr

Received: 18 July 2023 Accepted: 31 October 2023
Published online: 27 November 2023

complex formation and induce PCD, as well as the mechanisms by which the activation of multiple inflammasome sensors is regulated to effectively induce inflammatory cell death and inflammation, remain unknown.

Inflammatory cell death contributes to the release of proinflammatory cytokines, chemokines, and DAMPs during inflammation. Although inflammasome formation is inhibited after activation, the release of long-lived inflammasomes into the extracellular space has been reported [21–26]. Extracellular inflammasomes can propagate inflammatory responses through prion-like transmission, which is mediated by their engulfment by macrophages and amplifies inflammation [21–23]. Notably, increased extracellular inflammasome numbers have been observed in several disease models, including asthma [21], chronic obstructive pulmonary disease [22], pneumonia [22], and Alzheimer's disease [25]. However, the physiological roles of multiple PAMP- and DAMP-induced extracellular large multiprotein complexes and inflammation remain to be addressed.

Here, we discovered that the activation of multiple inflammasome sensors simultaneously leads to the initiation of multiple forms of PCD, and this phenomenon cannot be replicated by using a single ligand alone. We also observed that NLRP3, AIM2, NLRC4, and Pyrin, when simultaneously activated by specific ligands, form a large multiprotein complex with ASC, caspase-1, caspase-8, and RIPK3, resulting in the induction of various forms of PCD. These responses rely on the involvement of caspase-1, caspase-8, and RIPK3. Moreover, these large multiprotein complexes are released into the extracellular space, where they function as multiple inflammasomes. Interestingly, we found that the presence of multiple extracellular inflammasomes can trigger inflammation when they are engulfed by neighboring macrophages. Overall, our findings reveal a previously unknown regulatory connection and molecular interaction among inflammasome sensors, which leads to the formation of a multiprotein complex that includes multiple inflammasome sensors and regulators of cell death. These results offer a new perspective on the roles of these molecules in innate immunity and inflammatory cell death and present potential therapeutic targets for diseases mediated by NLRP3, AIM2, NLRC4, and Pyrin.

RESULTS

Canonical inflammasome ligands induce single inflammasome activation

To investigate whether the exposure of cells to either a single PAMP or a single DAMP can result in single inflammasome activation, we used well-established pure inflammasome ligands, including lipopolysaccharide (LPS) with ATP to activate the NLRP3 inflammasome [27], poly(dA:dT) to activate the AIM2 inflammasome [28, 29], flagellin to activate the NLRC4 inflammasome [30], and TcdB to activate the Pyrin inflammasome [31]. To study the role of NLRP3 inflammasome activation, we treated LPS-primed wild-type (WT), *Nlrp3*$^{-/-}$(NLRP3-deficient), *Aim2*$^{-/-}$, *Nlrc4*$^{-/-}$, and *Mefv*$^{-/-}$ bone marrow-derived macrophages (BMDMs) with ATP. We found that treatment of LPS-primed BMDMs with ATP induced the NLRP3-dependent cleavage of caspase-1, the release of the inflammasome-dependent cytokines IL-1β and IL-18, and cell death (Fig. S1A–E), suggesting that ATP is not sensed by other inflammasome sensors and that inflammasome activation in response to ATP occurs only through NLRP3. BMDMs that lacked AIM2 exhibited significantly decreased caspase-1 cleavage, IL-1β and IL-18 production, and cell death compared to WT BMDMs after poly(dA:dT) transfection (Fig. S1F–J). Flagellin transfection significantly decreased caspase-1 cleavage, IL-1β, and IL-18 release, and cell death in *Nlrc4*$^{-/-}$ BMDMs (Fig. S1K–O). We also found that TcdB-transfected BMDMs exhibited the pyrin-dependent cleavage of caspase-1, the release of the inflammasome-dependent cytokines IL-1β and IL-18, and cell death (Fig. S1P–T), suggesting that each pure inflammasome ligand induces specific inflammasome sensor-mediated inflammasome activation. Collectively, these results indicate that a single PAMP or DAMP can induce the activation of a single inflammasome.

Multiple inflammasome ligands promote multiple programmed cell death pathways

While there are several distinct inflammasome sensors, each of which responds to unique PAMPs or DAMPs and can form a caspase-1–activating multiprotein complex to drive pyroptosis, the presence of multiple PAMPs/DAMPs during infection or damage suggests that multiple inflammasome sensors can be engaged in a concerted effort to defend the host [7–11, 32]. As specific inflammasome sensor-mediated inflammasome activation was observed after treatment with each pure inflammasome ligand, we hypothesized that treatment with multiple pure inflammasome ligands could contribute to the simultaneous inflammasome sensor-mediated activation of multiple inflammasomes. We first examined the role of multiple PAMPs and DAMPs in inflammasome activation and cell death after treatment with multiple pure inflammasome ligands in a time-dependent manner. BMDMs from WT mice that were treated with a combination of multiple inflammasome ligands (LPS + ATP, poly (dA:dT), flagellin, and TcdB; Cocktail) exhibited increased cell death and IL-1β production compared to those that were treated with a single inflammasome ligand (LPS + ATP, poly (dA:dT), flagellin, or TcdB), and these effects occurred in a time-dependent manner (Fig. S2A–C). BMDMs from WT, *Nlrp3*$^{-/-}$, *Aim2*$^{-/-}$, *Nlrc4*$^{-/-}$, and *Mefv*$^{-/-}$ mice that were treated with a combination of multiple inflammasome ligands (Cocktail) exhibited comparable caspase-1 cleavage and IL-1β and IL-18 production to those observed in WT, *Nlrp3*$^{-/-}$, *Aim2*$^{-/-}$, *Nlrc4*$^{-/-}$, and *Mefv*$^{-/-}$ BMDMs (Fig. S2D–F); these results suggested that treatment with a combination of multiple inflammasome ligands results in multiple inflammasome activation.

In addition to activating more than one inflammasome, many pathogens induce multiple types of PCD, including pyroptosis, apoptosis, and necroptosis [12–19, 33, 34]. Although inflammasome activation is primarily associated with GSDMD-mediated pyroptosis, recent studies have found extensive crosstalk between PCD pathways and have demonstrated the contribution of inflammasome components as well as RIPK1, FADD, caspase-8, and RIPK3 in driving multiple inflammatory forms of PCD [11–20, 35–38]. To determine whether treatment with a combination of multiple inflammasome ligands induces multiple types of PCD, we characterized the cell death induced by a combination of multiple inflammasome ligands (LPS + ATP, poly(dA:dT), flagellin, and TcdB; Cocktail). In WT BMDMs, pure ligands of single inflammasomes, including LPS + ATP, poly(dA:dT), flagellin, or TcdB, activated the pyroptotic molecules caspase-1, GSDMD, and GSDME but not the cleavage of apoptotic caspase-8, caspase-3, and caspase-7 or the phosphorylation of the necroptotic molecule MLKL (Fig. 1A); these results indicated that a single inflammasome ligand is primarily associated with GSDMD-mediated pyroptosis. However, the combination of multiple inflammasome ligands (LPS + ATP, poly(dA:dT), flagellin, and TcdB; Cocktail) activated the pyroptotic molecules caspase-1, GSDMD, and GSDME, induced the cleavage of apoptotic caspase-8, caspase-3, and caspase-7, and promoted the phosphorylation of the necroptotic molecule MLKL in WT BMDMs (Fig. 1A). To determine what combination of PAMPs/DAMPs results in the initiation of apoptosis and necroptosis, we evaluated apoptosis and necroptosis after treatment with different combinations of three inflammasome ligands. Combinations of three inflammasome ligands (LPS + ATP + poly(dA:dT) + flagellin, LPS + ATP + poly(dA:dT) + TcdB, LPS + ATP + flagellin + TcdB, or poly(dA:dT) + flagellin + TcdB) reduced the activation of the apoptotic molecules caspase-8, caspase-3 and caspase-7 but

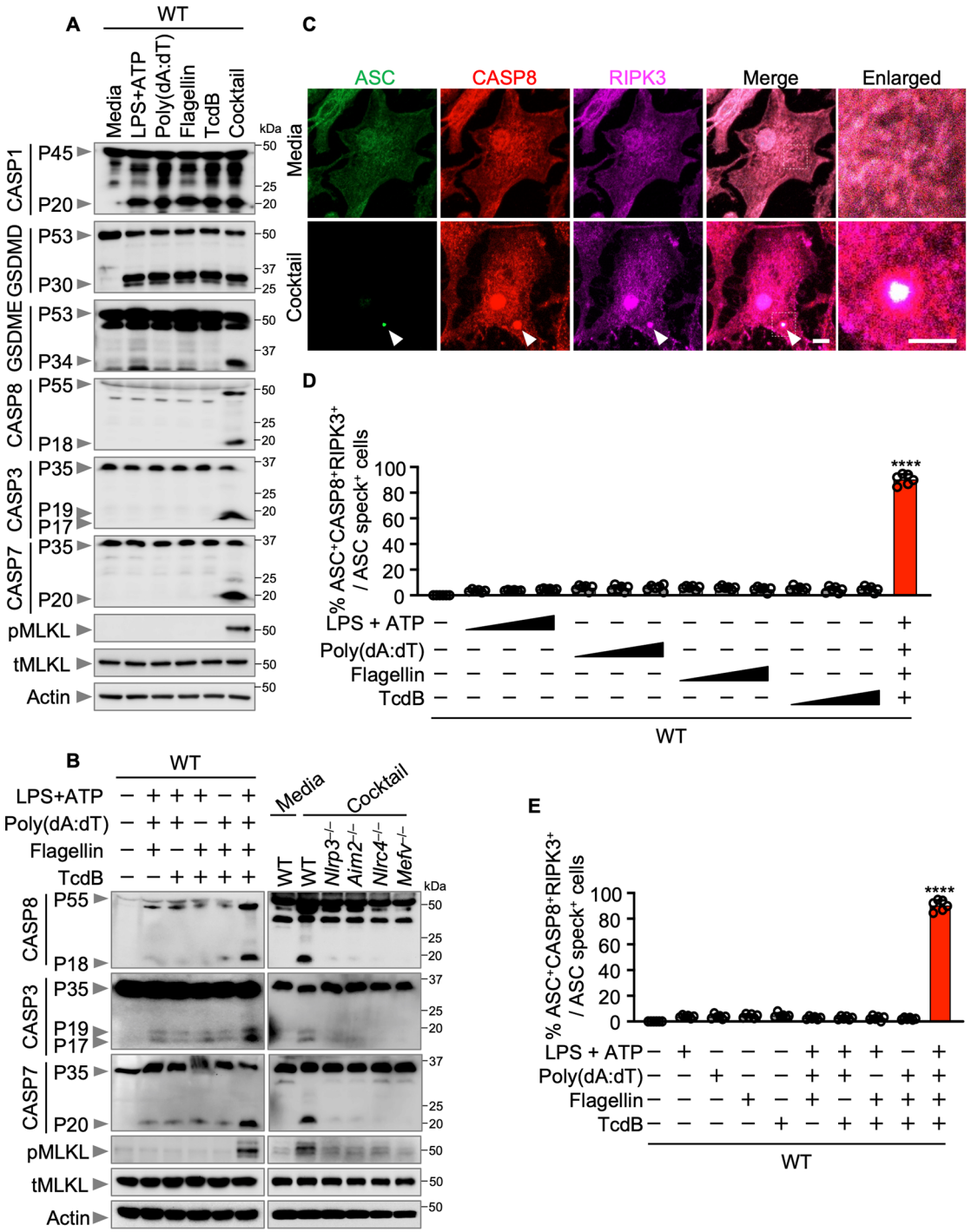

Fig. 1 Multiple inflammasome ligands promote multiple programmed cell death pathways. **A** Immunoblotting analysis of pro- (P45) and activated (P20) caspase-1 (CASP1), pro- (P53) and activated (P30) gasdermin D (GSDMD), pro- (P53) and activated (P34) gasdermin E (GSDME), pro- (P55) and cleaved (P18) caspase-8 (CASP8), pro- (P35) and cleaved (P17/P19) caspase-3 (CASP3), pro- (P35) and cleaved (P20) caspase-7 (CASP7), phosphorylated MLKL (pMLKL), total MLKL (tMLKL) expression wild type (WT) bone marrow-derived macrophages (BMDMs) treated with a single ligand (LPS + ATP, poly(dA:dT), flagellin, or TcdB) or a combination of LPS + ATP, poly(dA:dT), flagellin, and TcdB (Cocktail). **B** Immunoblotting analysis of CASP8, CASP3, CASP7, pMLKL, and tMLKL expression in WT BMDMs treated with the indicated treatments or in WT, *Nlrp3*$^{-/-}$, *Aim2*$^{-/-}$, *Nlrc4*$^{-/-}$, or *Mefv*$^{-/-}$ BMDMs treated with the Cocktail. Data are representative of at least three independent experiments (**A**, **B**). **C** Immunofluorescence images of WT BMDMs 6 h after Cocktail treatment. Scale bars, 5 μm. Arrowheads indicate ASC specks. Images are representative of three independent experiments. **D** Quantification of the percentage of cells with ASC^{+}CASP8^{+}RIPK3^{+} specks among the ASC speck^{+} cells after treatment with varying concentrations of the individual ligands: 500 ng/ml LPS + 1 μM, 5 μM, or 25 μM ATP; 0.2 ng, 1 ng, or 5 ng poly(dA:dT); 2 ng, 10 ng, or 50 ng flagellin; 0.1 μg/ml, 0.5 μg/ml, or 2.5 μg/ml TcdB; or Cocktail (500 ng/ml LPS + 5 μM ATP + 1 ng poly(dA:dT) + 10 ng flagellin + 0.5 μg/ml TcdB). Data are mean ± s.e.m. ****$P < 0.0001$ (one-way ANOVA with Dunnett's multiple comparisons test; $n = 6$ from three biologically independent samples). **E** Quantification of the percentage of cells with ASC^{+}CASP8^{+}RIPK3^{+} specks among the ASC speck^{+} WT BMDMs after the indicated treatment (5 μM ATP, 1 ng poly(dA:dT), 10 ng flagellin, and/or 0.5 μg/ml TcdB). Data are mean ± s.e.m. ****$P < 0.0001$ (one-way ANOVA with Dunnett's multiple comparisons test; $n = 6$ from three biologically independent samples)

not the necroptotic molecule MLKL compared to the Cocktail treatment (LPS + ATP + poly (dA:dT) + flagellin + TcdB; Cocktail) (Fig. 1B). Furthermore, the Cocktail reduced the activation of apoptotic molecules, including caspase-8, caspase-3, and caspase-7, as well as the necroptotic molecule MLKL in *Nlrp3*$^{-/-}$, *Aim2*$^{-/-}$, *Nlrc4*$^{-/-}$, and *Mefv*$^{-/-}$ BMDMs compared to the degree of their activation in WT BMDMs (Fig. 1B), suggesting that a combination of four inflammasome ligands (LPS + ATP + poly (dA:dT) + flagellin + TcdB) can uniquely induce the formation of multi-protein complexes and initiate pyroptosis, apoptosis, and necroptosis.

Multiple inflammasome ligands induce the assembly of complexes that include NLRP3, AIM2, NLRC4, and Pyrin

Next, we sought to understand the molecular relationship between inflammasome sensors, including NLRP3, AIM2, NLRC4, and Pyrin, that are involved in inducing inflammatory cell death after treatment with multiple inflammasome ligands. We hypothesized that these molecules are part of the molecular scaffold that allows the simultaneous engagement of key molecules that contribute to pyroptosis, apoptosis, and necroptosis [11, 12, 14, 35, 39–41]. We observed the interactions among endogenous ASC and NLRP3, AIM2, NLRC4, Pyrin, caspase-8, and RIPK3 using immunoprecipitation following Cocktail treatment (Fig. 2A). However, ASC interacted with a single inflammasome sensor but not with other inflammasome sensors, caspase-8, and RIPK3, in response to specific single inflammasome ligands (Fig. 2A). Loss of NLRP3, AIM2, NLRC4, or Pyrin completely abolished the interactions of caspase-8 and RIPK3 with ASC specks after Cocktail treatment (Fig. 2B). ASC specks colocalized with NLRP3, AIM2, NLRC4, and Pyrin as well as caspase-8 and RIPK3 in response to Cocktail treatment (LPS + ATP, poly (dA:dT), flagellin, and TcdB) but not in response to treatment with a single inflammasome ligand (LPS + ATP, poly (dA:dT), flagellin, or TcdB) (Fig. 2C–E). Furthermore, the loss of NLRP3, AIM2, NLRC4, or Pyrin completely abolished the colocalization of caspase-8 and RIPK3 with ASC specks after Cocktail treatment (Fig. 2F, G). Notably, the colocalization of NLRP3, AIM2, NLRC4, and Pyrin as well as caspase-8 and RIPK3 with ASC specks persisted in *Nlrp1a*$^{-/-}$, *Nlrp1b*$^{-/-}$, and *Casp11*$^{-/-}$ iBMDMs (Fig. S3A, B), indicating that noncanonical inflammasome sensors, namely, NLRP1 and caspase-11, are not essential for the recruitment of caspase-8 and RIPK3 to the ASC speck after stimulation with multiple inflammasome ligands. Furthermore, ASC specks colocalized with NLRP3, AIM2, NLRC4, and Pyrin, as well as caspase-8 and RIPK3, in WT BMDMs after exposure to both the LPS + nigericin Cocktail (alternative NLRP3 inflammasome ligand) and the LPS + ATP Cocktail (conventional NLRP3 inflammasome ligand) (Fig. S3C, D); these results indicated that treatment with various inflammasome ligands, such as LPS + nigericin in lieu of LPS + ATP, remains effective in recruiting caspase-8 and RIPK3 to the ASC speck. To mimic the Cocktail-induced simultaneous activation of multiple inflammasomes, we evaluated the colocalization of the ASC speck, NLRP3, AIM2, NLRC4, and Pyrin after coinfection with influenza A virus (IAV) (a ligand of the NLRP3 inflammasome) and HSV1 (a ligand of the AIM2 and Pyrin inflammasomes) in conjunction with flagellin (an activator of the NLRC4 inflammasome). ASC specks colocalized with NLRP3, AIM2, NLRC4, and Pyrin in WT BMDMs after coinfection with IAV and HSV1 along with flagellin (Fig. S3E). However, we observed that ASC specks did not colocalize with NLRP3, AIM2, NLRC4, or Pyrin after individual infection/treatment (IAV, HSV1, or flagellin) or double infection/treatment (IAV + HSV1, IAV + flagellin, or HSV1 + flagellin) (Fig. S3E); these results indicated that pathogen cocktails can compensate for the phenotypic effects exerted by multiple inflammasome ligands. Collectively, these data indicate that NLRP3, AIM2, NLRC4, and Pyrin are all members of the multiprotein complex that forms with ASC in response to multiple PAMPs and DAMPs.

Multiple inflammasome ligands promote multiple programmed cell death pathways in a RIPK3/caspase-8-dependent manner

Notably, the innate immune sensor or caspase-8/RIPK3 axis drives multiple forms of inflammatory PCD in the presence of multiple PAMPs/DAMPs during live pathogen infection or damage [11, 13, 14, 20, 35]. As previously reported [11, 13], IAV and HSV1 activate key molecules that are involved in the pyroptotic, apoptotic, and necroptotic pathways in WT BMDMs (Fig. S4A–C). However, we observed a complete loss of activation of the pyroptotic molecules caspase-1 and GSDMD and the apoptotic molecules caspase-8, caspase-3, and caspase-7 as well as a lack of phosphorylation of the necroptotic molecule MLKL in *Zbp1*$^{-/-}$ or *Aim2*$^{-/-}$ BMDMs compared to WT BMDMs after IAV or HSV1 infection, respectively (Fig. S4A–C). We also observed interactions of endogenous ASC with NLRP3, ZBP1, caspase-8, and RIPK3 during IAV infection and interactions of endogenous ASC with AIM2, Pyrin, ZBP1, caspase-8, and RIPK3 during HSV1 infection using immunoprecipitation, whereas these interactions were completely abolished in *Zbp1*$^{-/-}$ and *Aim2*$^{-/-}$ BMDMs (Fig. S4D). Furthermore, ASC specks colocalized with caspase-8 or RIPK3 in a ZBP1-dependent manner during IAV infection and in an AIM2-dependent manner during HSV1 infection (Fig. S4E); these results suggested that innate immune sensors, including ZBP1 or AIM2, promote inflammatory cell death in response to IAV or HSV1 infection, respectively. To inhibit caspase-8 and RIPK3 activation, we used Z-IETD-FMK to inhibit caspase-8 and GSK-872 to inhibit RIPK3. We observed a complete loss of activation of the pyroptotic, apoptotic, and necroptotic pathways in after treatment with Z-IETD-FMK and GSK-872 during IAV and HSV1 infection (Fig. S4C); these results indicated that caspase-8 and RIPK3 are key regulators of inflammatory cell death in response to IAV and HSV1 infection.

To determine whether the caspase-8/RIPK3 axis drives multiple forms of inflammatory PCD in the presence of multiple PAMPs/DAMPs, we next used Z-IETD-FMK and GSK-872 to inhibit the activation of caspase-8 and RIPK3, respectively. We found that the Cocktail induced cell death, IL-1β release, activation of key molecules involved in the pyroptotic, apoptotic, and necroptotic pathways and complete loss of activation in WT BMDMs that were treated with Z-IETD-FMK and GSK-872 (Fig. 3A–D). To further confirm that caspase-8 and RIPK3 work cooperatively in these processes, we established *Ripk3*$^{-/-}$*Casp8*$^{-/-}$ iBMDMs. Treatment of *Ripk3*$^{-/-}$*Casp8*$^{-/-}$ iBMDMs with the Cocktail resulted in the complete abrogation of cell death, IL-1β release, and activation of key molecules involved in the pyroptotic, apoptotic, and necroptotic pathways (Fig. 3E–H). We also observed interactions of endogenous RIPK3 with NLRP3, AIM2, NLRC4, Pyrin, caspase-8, and ASC after Cocktail treatment, and these interactions occurred in a RIPK3/caspase-8-dependent manner (Fig. S5A). Furthermore, ASC specks colocalized with caspase-8 or RIPK3 in WT BMDMs (Fig. S5B–D) and WT iBMDMs (Fig. S5E–G) after Cocktail treatment. However, ASC specks did not colocalize with caspase-8 or RIPK3 in WT BMDMs treated with Z-IETD-FMK and GSK-872 or *Ripk3*$^{-/-}$*Casp8*$^{-/-}$ iBMDMs treated with the Cocktail (Fig. S5B–G). Collectively, these results indicate that multiple PAMPs/DAMPs promote multiple pathways of programmed inflammatory cell death in a RIPK3/caspase-8-dependent manner.

The catalytic activity of caspase-1 is not needed for the recruitment of caspase-8 and RIPK3 to ASC specks

In response to multiple PAMPs/DAMPs during infection, caspase-1 is a critical component of the multiprotein complex, and it interacts with ASC to induce inflammatory cell death [11]. We initially found that the Cocktail induced the activation of key molecules involved in the pyroptotic, apoptotic, and necroptotic pathways in WT BMDMs and completely blocked this activation in *Casp1*$^{-/-}$ BMDMs (Fig. 4A). To determine whether the catalytic activity of caspase-1 is needed for the recruitment of multiprotein complexes to ASC specks, we next used VX-765 and Ac-YVAD-cmk,

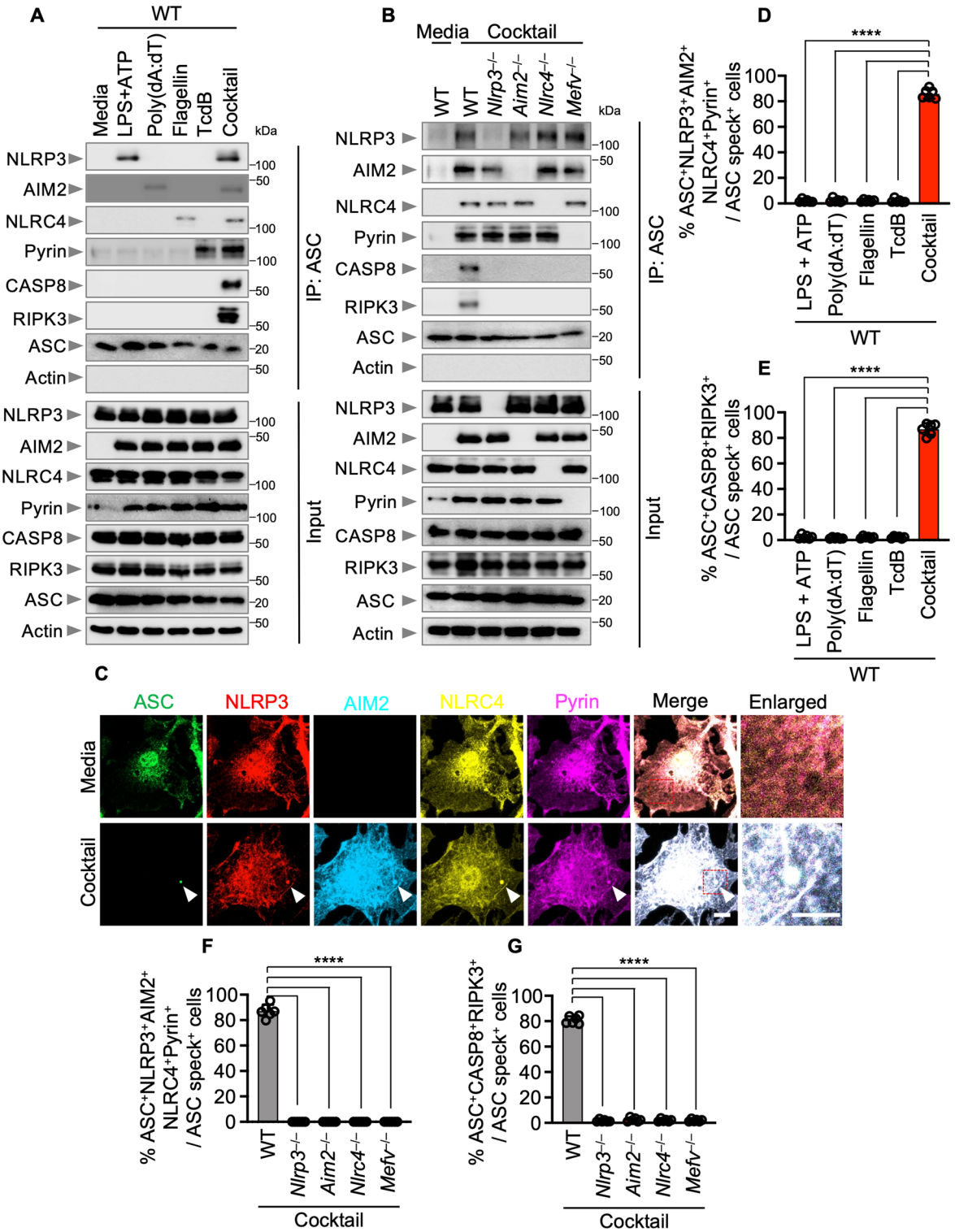

Fig. 2 Multiple inflammasome ligands induce the assembly of integrated NLRP3, AIM2, NLRC4, and Pyrin complexes. **A** Immunoprecipitation (IP) of wild-type (WT) bone marrow-derived macrophages (BMDMs) with anti-ASC antibodies after treatment with LPS + ATP, poly(dA:dT), flagellin, or TcdB alone or treatment with a combination of LPS + ATP, poly(dA:dT), flagellin, and TcdB (Cocktail). Data are representative of three independent experiments. **B** IP of WT, *Nlrp3*$^{-/-}$, *Aim2*$^{-/-}$, *Nlrc4*$^{-/-}$, or *Mefv*$^{-/-}$ BMDMs with anti-ASC antibodies after Cocktail treatment. Data are representative of three independent experiments. **C** Immunofluorescence images of WT BMDMs 6 h after Cocktail treatment. Scale bars, 5 μm. Arrowheads indicate ASC specks. Images are representative of three independent experiments. Quantification of the percentage of cells with ASC^{+}NLRP3^{+}AIM2^{+}NLRC4^{+}Pyrin^{+} specks among the ASC speck^{+} WT BMDMs (**D**) or cells with ASC^{+}CASP8^{+}RIPK3^{+} specks among the ASC speck^{+} WT BMDMs (**E**) after the indicated treatment. Quantification of the percentage of cells with ASC^{+}NLRP3^{+}AIM2^{+}NLRC4^{+}Pyrin^{+} specks among the ASC speck^{+} cells (**F**) or ASC^{+}CASP8^{+}RIPK3^{+} specks among the ASC speck^{+} cells (**G**) after treatment of the indicated BMDMs with the Cocktail. Data are mean ± s.e.m. ns, not significant, ****$P < 0.0001$ (one-way ANOVA with Dunnett's multiple comparisons test; $n = 6$ from three biologically independent samples) (**D**, **E**, **F**, **G**)

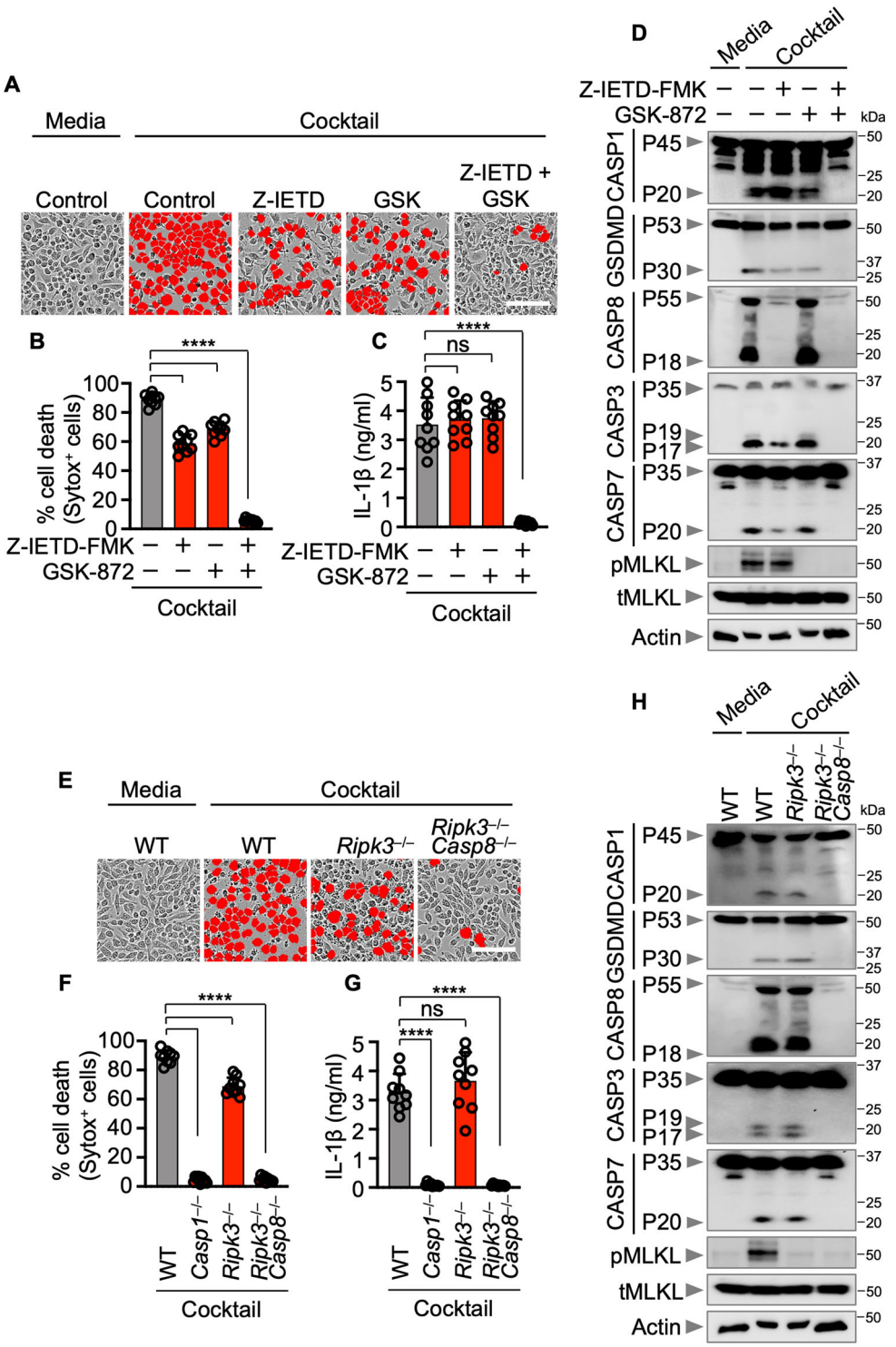

Fig. 3 Multiple inflammasome ligands promote multiple programmed cell death pathways in a RIPK3/caspase-8-dependent manner. **A** Cell death of wild-type (WT) bone marrow-derived macrophages (BMDMs) treated with Z-IETD-FMK, GSK-872, or a combination of Z-IETD-FMK and GSK-872 after treatment with the combination of combination LPS + ATP, poly(dA:dT), flagellin, and TcdB (Cocktail). **B** Quantification of cell death in (**A**). **C** Assessment of IL-1β levels. **D** Immunoblotting analysis of pro- (P45) and activated (P20) caspase-1 (CASP1), pro- (P53) and activated (P30) gasdermin D (GSDMD), pro- (P55) and cleaved (P18) caspase-8 (CASP8), pro- (P35) and cleaved (P17/P19) caspase-3 (CASP3), pro- (P35) and cleaved (P20) caspase-7 (CASP7), phosphorylated MLKL (pMLKL), total MLKL (tMLKL) expression in WT BMDMs treated with Z-IETD-FMK, GSK-872, or a combination of Z-IETD-FMK and GSK-872 after Cocktail treatment. **E** Cell death in WT, *Casp1*$^{-/-}$, *Ripk3*$^{-/-}$, and *Ripk3*$^{-/-}$*Casp8*$^{-/-}$ immortalized bone marrow-derived macrophages (iBMDMs) after Cocktail treatment. **F** Quantification of cell death in (**E**). **G** Assessment of IL-1β levels. **H** Immunoblotting analysis of CASP1, GSDMD, CASP8, CASP3, CASP7, pMLKL, and tMLKL expression in WT, *Casp1*$^{-/-}$, *Ripk3*$^{-/-}$, and *Ripk3*$^{-/-}$*Casp8*$^{-/-}$ iBMDMs after Cocktail treatment. Images are representative of at least three independent experiments; red indicates dead cells; scale bar, 50 μm (**A**, **E**). Data are mean ± s.e.m. ****$P < 0.0001$ (one-way ANOVA with Dunnett's multiple comparisons test; $n = 9$ from three biologically independent samples) (**B**, **C**, **F**, **G**). Data are representative of at least three independent experiments (**D**, **H**)

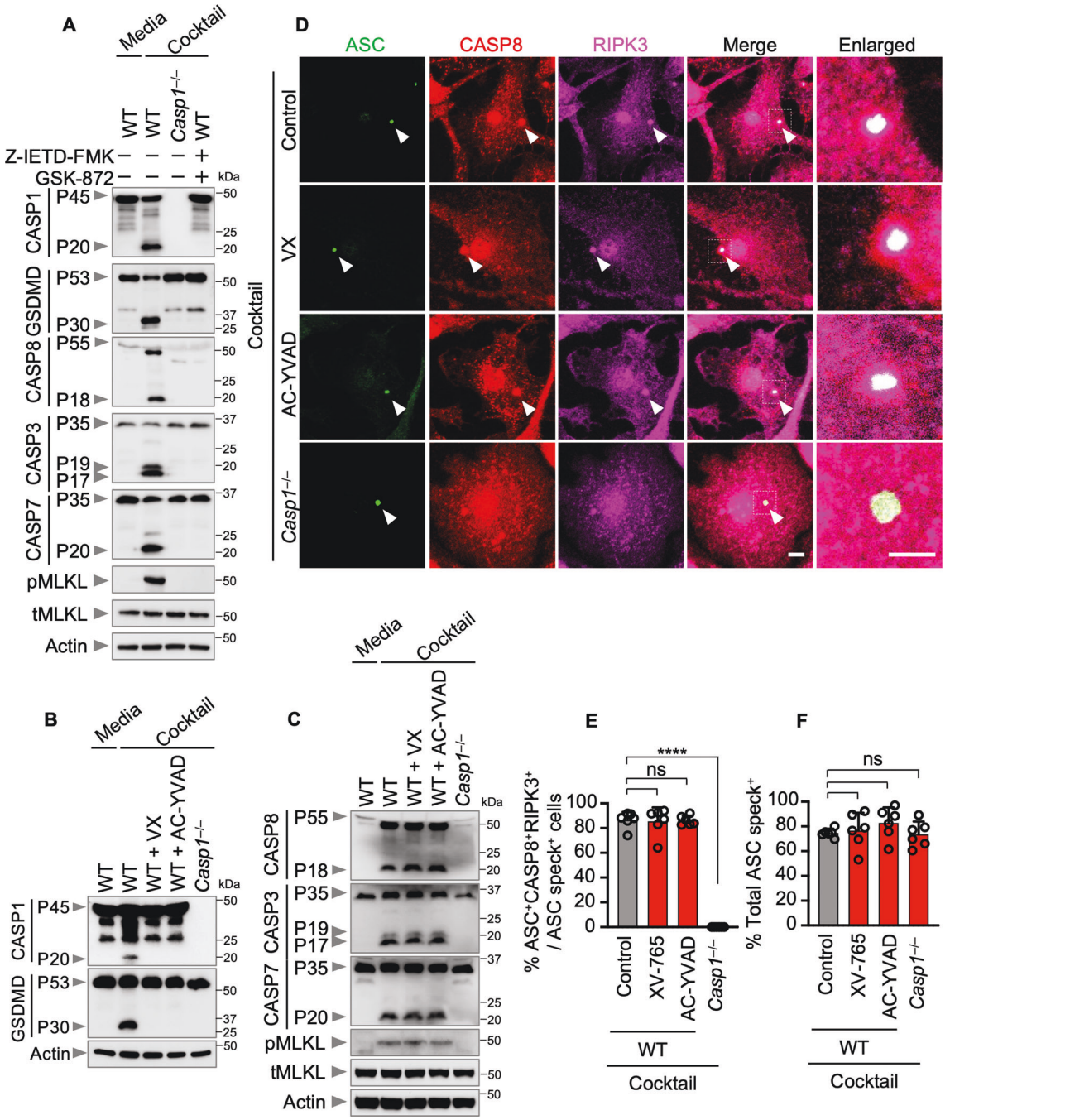

Fig. 4 Catalytic activity of caspase-1 is not needed for recruitment of caspase-8 and RIPK3 to ASC speck. **A** Immunoblotting analysis of pro- (P45) and activated (P20) caspase-1 (CASP1), pro- (P53) and activated (P30) gasdermin D (GSDMD), pro- (P55) and cleaved (P18) caspase-8 (CASP8), pro- (P35) and cleaved (P17/P19) caspase-3 (CASP3), pro- (P35) and cleaved (P20) caspase-7 (CASP7), phosphorylated MLKL (pMLKL), total MLKL (tMLKL) expression in wild type (WT), *Casp1*$^{-/-}$, and WT bone marrow-derived macrophages (BMDMs) treated with the combination of Z-IETD-FMK and GSK-872 after Cocktail treatment. **B** Immunoblotting analysis of CASP1 and GSDMD expression in Cocktail-treated WT, *Casp1*$^{-/-}$, and WT BMDMs treated with either VX-765 or Ac-YAVD-cmk. **C** Immunoblotting analysis of pro- (P55) and cleaved (P18) caspase-8 (CASP8), pro- (P35) and cleaved (P17/P19) caspase-3 (CASP3), pro- (P35) and cleaved (P20) caspase-7 (CASP7), phosphorylated MLKL (pMLKL), and total MLKL (tMLKL) expression in WT, *Casp1*$^{-/-}$, and WT BMDMs treated with either VX-765 or Ac-YAVD-cmk after Cocktail treatment. **D** Immunofluorescence images of the indicated BMDMs 6 h after Cocktail treatment. Scale bars, 5 μm. Arrowheads indicate ASC specks. Images are representative of three independent experiments. **E** Quantification of the percentage of cells with ASC specks among total cells in the indicated groups of BMDM after Cocktail treatment. **F** Quantification of the percentage of cells with ASC^{+}CASP8^{+}RIPK3^{+} specks among the ASC speck^{+} cells in the indicated groups of BMDMs after Cocktail treatment. Data are representative of at least three independent experiments (**A**, **B**, **C**). Data are mean ± s.e.m. ns, not significant, ****$P < 0.0001$ (one-way ANOVA with Dunnett's multiple comparisons test; $n = 6$ from 3 biologically independent samples) (**D**, **E**, **F**)

typical inhibitors of the catalytic activity of caspase-1. We observed a loss of the activation of pyroptotic molecules, including caspase-1 and GSDMD, but not apoptotic molecules, including caspase-8, caspase-3, and caspase-7, and the necroptotic molecule MLKL was inhibited in WT BMDMs treated with VX-765 or Ac-YVAD-cmk (Fig. 4B, C). Based on the VX-765 and Ac-YVAD-cmk treatment conditions, we next evaluated the colocalization of ASC specks, caspase-8, and RIPK3 to determine whether the active form of caspase-1 is needed for the recruitment of caspase-8 and RIPK3. ASC specks colocalized with caspase-8 and RIPK3 in WT BMDMs treated with both VX-765 and Ac-YVAD-cmk. However, ASC specks did not colocalize with caspase-8 and RIPK3 in *Casp1*$^{-/-}$ BMDMs after Cocktail treatment (Fig. 4D–F). These results indicate that the catalytic activity of caspase-1 is not needed for the recruitment of caspase-8 and RIPK3 to ASC specks, but pro-caspase-1 is needed for multiprotein complex formation.

Activation of the multiple inflammasome sensor-containing multiprotein complex induces the release of NLRP3, AIM2, NLRC4, Pyrin, and ASC

Inflammasome-derived ASC specks have been determined to be released from cells into the extracellular space; furthermore, extracellular ASC can propagate inflammatory responses through prion-like transmission that is mediated by their engulfment by neighboring macrophages [21–23, 25, 26]. To gain insight into the kinetics of ASC speck formation and cell death, we used BMDMs derived from ASC-citrine mice [42] and performed live-cell imaging with propidium iodide (PI) staining. Consistent with the live-cell imaging observations, after ASC speck-positive cells were treated with the Cocktail, the cells exhibited PI-positive staining (Fig. 5A–C), suggesting that ASC speck formation is closely followed by loss of cell membrane integrity and cell death.

To determine whether Cocktail-induced ASC specks are released into the extracellular space, we stained ASC, as the hallmark of the multiprotein complex, and tubulin, as a marker of the cell cytoplasm. ASC specks whose formation was induced by the Cocktail were released into the extracellular space in a time-dependent manner (Fig. 5D, E). To investigate the components of the multiprotein complex that are released into the extracellular space, cell-free extracellular ASC-citrine specks were purified from BMDMs isolated from ASC-citrine mice after Cocktail treatment using Percoll gradient centrifugation (Fig. S6A, B). Simultaneous activation of the inflammasome using the Cocktail resulted in the release of mature caspase-1 p20 as well as the inflammasome components NLRP3, AIM2, NLRC4, Pyrin, ASC, and pro-caspase-1 (p45) into the extracellular space (Fig. 5F). Cocktail treatment failed to induce the extracellular release of ASC specks by *Casp1*$^{-/-}$ and WT BMDMs after Z-IETD-FMK and GSK-872 treatment (Fig. 5G). Activation of the inflammasome using a single inflammasome ligand resulted in the release of the corresponding specific inflammasome sensor (NLRP3, AIM2, NLRC4, or Pyrin) and ASC into the extracellular space (Fig. 5H). We also observed a complete inhibition of the extracellular release of NLRP3, AIM2, NLRC4, Pyrin, and ASC from *Casp1*$^{-/-}$ and WT BMDMs after Z-IETD-FMK and GSK-872 treatment (Fig. 5I). These results indicate that the activation of multiple inflammasomes induces the release of NLRP3, AIM2, NLRC4, Pyrin, and ASC.

Extracellular multiple inflammasome particle-driven inflammation depends on caspase-1 or the caspase-8/RIPK3 axis

Emerging evidence indicates that ASC specks are released into the extracellular space where they are engulfed by neighboring macrophages to induce sterile inflammation through a prion-like mechanism in the absence of any allergens or infectious agents [21–23]. To examine the phagocytosis of ASC specks by macrophages, WT airway macrophages were incubated with purified extracellular ASC-citrine specks and stained with Alexa Fluor 568 phalloidin to label the cytoplasm. We found that ASC-citrine specks were engulfed by WT airway macrophages (Fig. S6C), and this engulfment was associated with substantial IL-1β secretion (Fig. S6D); these results suggested that extracellular ASC specks are internalized by neighboring phagocytic cells to induce an inflammatory response.

We extended our findings to an in vivo setting and monitored the changes in the body weight of WT, *Casp1*$^{-/-}$, *Nlrp3*$^{-/-}$, *Aim2*$^{-/-}$, *Nlrc4*$^{-/-}$, or *Mefv*$^{-/-}$ mice after the intranasal administration of purified ASC-citrine specks from cells treated with single inflammasome ligands. The administration of purified ASC-citrine specks from LPS + ATP-treated cells resulted in decreased body weight in WT mice. However, the weight of the *Nlrp3*$^{-/-}$ and *Casp1*$^{-/-}$ mice recovered compared with that of the WT mice after the intranasal administration of purified ASC-citrine specks from LPS + ATP-treated cells (Fig. 6A). Similarly, purified ASC-citrine specks from poly(dA:dT)-treated cells decreased body weight in an AIM2- or caspase-1-dependent manner (Fig. 6B). The body weights of *Nlrc4*$^{-/-}$ and *Casp1*$^{-/-}$ mice recovered compared with that of WT mice after the intranasal administration of purified ASC-citrine specks from flagellin-treated cells (Fig. 6C). The weight of *Mefv*$^{-/-}$ and *Casp1*$^{-/-}$ mice also recovered compared with that of WT mice after the intranasal administration of purified ASC-citrine specks from TcdB-treated cells (Fig. 6D), and these results indicated that single inflammasome sensors and caspase-1 are needed for changes in body weight in response to single inflammasome ligand-induced extracellular ASC specks.

We next monitored the changes in the body weight of WT, *Nlrp3*$^{-/-}$, *Aim2*$^{-/-}$, *Nlrc4*$^{-/-}$, and *Mefv*$^{-/-}$ mice after the intranasal administration of purified ASC-citrine specks from multiple inflammasome ligand-treated cells. The administration of purified ASC specks from Cocktail-treated cells decreased the body weight of WT mice, whereas the weight loss was comparable in WT, *Nlrp3*$^{-/-}$, *Aim2*$^{-/-}$, *Nlrc4*$^{-/-}$, and *Mefv*$^{-/-}$ mice (Fig. 7A); these results suggested that loss of a single inflammasome sensor did not affect the changes in body weight caused by purified ASC specks from Cocktail-treated cells. The weight of *Casp1*$^{-/-}$ mice recovered compared with that in the WT mice in the second week after the intranasal administration of purified ASC specks from Cocktail-treated cells (Fig. 7B). To understand the potential impact of blocking the caspase-8/RIPK3 axis during disease, we intranasally treated WT mice with Z-IETD-FMK and GSK-872 24 h before administering purified extracellular ASC-citrine specks. Although the weight loss in WT mice was comparable to that in WT mice treated with Z-IETD-FMK or GSK-872 alone, WT mice treated with a combination of Z-IETD-FMK and GSK-872 exhibited a recovery in weight after the intranasal administration of purified ASC specks from Cocktail-treated cells (Fig. 7C), suggesting that caspase-1 and the caspase-8/RIPK3 axis are key components of this multiprotein complex and are critical regulators of changes in body weight in response to purified ASC specks from Cocktail-treated cells.

Bronchoalveolar lavage fluid (BALF) was used to investigate extracellular ASC speck-driven inflammation. The amount of IL-1β in the BALF from *Casp1*$^{-/-}$ mice or WT mice that were treated with Z-IETD-FMK and GSK-872 was reduced compared to that from WT mice (Fig. 7D). To quantify the extent of leukocyte infiltration, we further determined the number of leukocytes in BALF using an anti-Gr-1 antibody to label granulocytes. As expected, the number of infiltrating leukocytes in *Casp1*$^{-/-}$ or WT mice treated with Z-IETD-FMK and GSK-872 was lower than that in WT mice (Fig. 7E), indicating that extracellular multiple inflammasome particle-driven inflammation depends on caspase-1 or the caspase-8/RIPK3 axis.

We also found that the weight of WT mice that were treated with a combination of Z-IETD-FMK and GSK-872 recovered after the intranasal administration of purified ASC-citrine specks from cells treated with multiple inflammasome ligands (LPS + ATP, poly(dA:dT), flagellin, and TcdB; Cocktail). However, WT mice treated

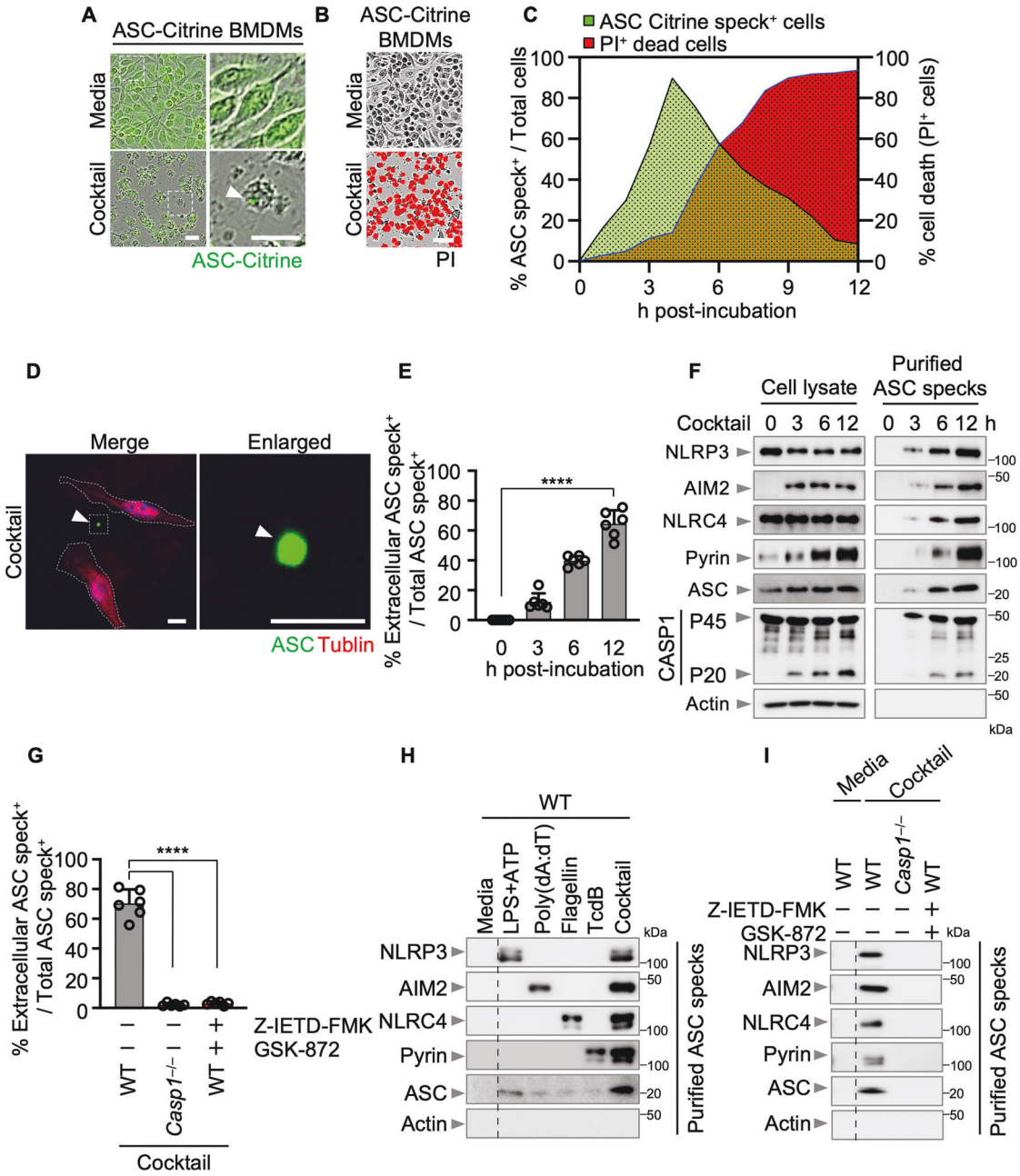

Fig. 5 Activation of the multiple inflammasome sensor-mediated multiprotein complex formation induces the release of NLRP3, AIM2, NLRC4, Pyrin, and ASC. Live-cell imaging of ASC-citrine bone marrow-derived macrophages (BMDMs) after treatment with the combination of LPS + ATP, poly(dA:dT), flagellin, and TcdB (Cocktail). Arrowheads indicate ASC specks (**A**). Red indicates dead cells (**B**). Scale bar, 25 μm. Quantification of ASC specks and cell death in ASC-citrine BMDMs over time after Cocktail treatment (**C**). Data are representative of at least three independent experiments. **D** Immunofluorescence images of WT BMDMs after Cocktail treatment. Scale bars, 5 μm. Arrowheads indicate extracellular ASC specks. Images are representative of three independent experiments. **E** Quantification of the percentage of extracellular ASC specks among total ASC specks in WT BMDMs over time after Cocktail treatment. **F** Immunoblotting analysis of NLRP3, AIM2, NLRC4, Pyrin, ASC, pro-caspase-1 (CASP1; P45), and cleaved CASP1 (P20) expression in cell lysates of WT BMDMs or 1×10^7 particles of purified ASC-Citrine specks obtained using a Percoll gradient after Cocktail treatment. **G** Quantification of the percentage of extracellular ASC specks among total ASC specks in WT, *Casp1*$^{-/-}$, or WT BMDMs treated with Z-IETD-FMK and GSK-872 after Cocktail treatment. **H** Immunoblotting analysis of NLRP3, AIM2, NLRC4, Pyrin, and ASC expression in 1×10^7 particles of purified ASC-Citrine specks after the indicated treatment. **I** Immunoblotting analysis of NLRP3, AIM2, NLRC4, Pyrin, and ASC expression in 1×10^7 particles of purified ASC-Citrine specks after Cocktail treatment. Data are mean ± s.e.m. ****$P < 0.0001$ (one-way ANOVA with Dunnett's multiple comparisons test; $n = 6$ from three biologically independent samples) (**E**, **G**). Data are representative of three independent experiments (**F**, **H**, **I**)

with a combination of Z-IETD-FMK and GSK-872 show decreased body weight after the intranasal administration of purified ASC-citrine specks from cells treated with single inflammasome ligands (LPS + ATP, poly (dA:dT), flagellin, or TcdB) (Fig. 7F); these results suggested that in response to treatment with multiple inflammasome ligands (LPS + ATP, poly (dA:dT), flagellin, and TcdB; Cocktail), a complex with more molecular components than the traditional inflammasome (inflammasome sensor-ASC-CASP1) is formed, and this complex includes NLRP3, AIM2, NLRC4, Pyrin, ASC, caspase-8, and RIPK3.

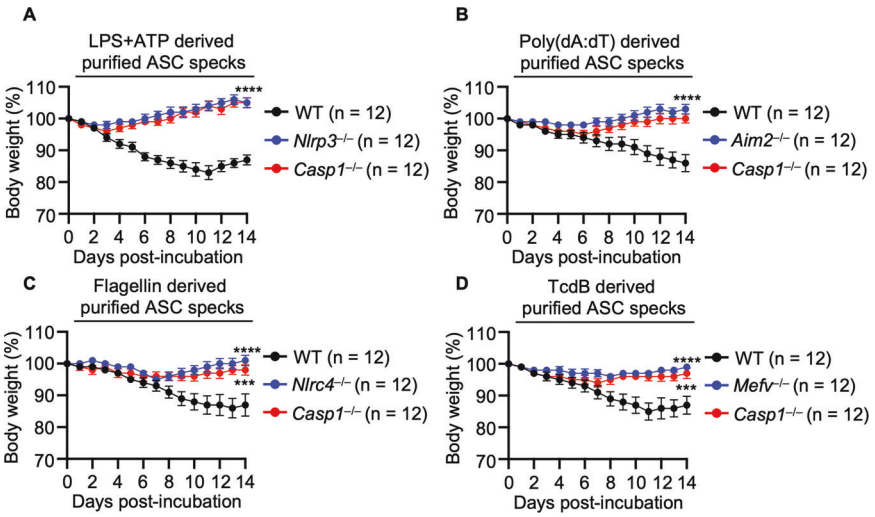

Fig. 6 Single inflammasome sensors and caspase-1 are needed for changes in body weight in response to extracellular ASC specks induced by a single inflammasome ligand. **A** Body weights of 6- to 8-week-old wild-type (WT), *Nlrp3*$^{-/-}$, or *Casp1*$^{-/-}$ mice after the intranasal administration of 5×10^6 particles of purified ASC-Citrine specks after LPS + ATP treatment. **B** Body weights of 6- to 8-week-old WT, *Aim2*$^{-/-}$, or *Casp1*$^{-/-}$ mice after the intranasal administration of 5×10^6 particles of purified ASC-Citrine specks after poly(dA:dT) treatment. **C** Body weights of 6- to 8-week-old WT, *Nlrc4*$^{-/-}$, or *Casp1*$^{-/-}$ mice after the intranasal administration of 5×10^6 particles of purified ASC-Citrine specks after flagellin treatment. **D** Body weights of 6- to 8-week-old WT, *Mefv*$^{-/-}$, or *Casp1*$^{-/-}$ mice after the intranasal administration of 5×10^6 particles of purified ASC-Citrine specks after TcdB treatment. Data are shown as the mean ± SEM (**A**, **B**, **C**, **D**). Data are pooled from three independent experiments (**A**, **B**, **C**, **D**)

DISCUSSION

Many pathogens induce multiple forms of inflammatory PCD, including pyroptosis, apoptosis, and necroptosis [12–19]. Recent studies have shown extensive crosstalk among these forms of PCD [12, 13, 16–19], establishing the concept of PANoptosis [11, 13, 14, 35–38]. Although inflammasome activation is primarily associated with GSDMD-mediated pyroptosis, the contribution of inflammasome components to PANoptosis is now emerging [11, 13, 14, 35–38]. PANoptosis acts as a double-edged sword in host defense and offense during live-pathogen infections. For instance, PANoptosis contributes to the inflammatory response and is needed to protect the host against IAV, HSV1, and *Francisella* infection [11, 13, 20]. However, PANoptosis contributes to cytokine storms, tissue damage, and ultimately death in response to severe acute respiratory syndrome coronavirus 2 and mouse hepatitis virus infection [20, 35].

Here, we discovered that NLRP3, AIM2, NLRC4, and Pyrin form a multiprotein complex via interactions with ASC to induce PANoptosis in response to multiple inflammasome ligands. Loss of caspase-1 or caspase-8/RIPK3 induces the complete loss of PANoptosis during this treatment. This activity was specific to a combination of multiple inflammasome ligands (LPS + ATP, poly (dA:dT), flagellin, and TcdB; Cocktail) and could not be mimicked by treatments with a single pure ligand, suggesting that a combination of PAMPs may be needed to regulate the multi-protein complex and PANoptosis.

Emerging genetic and biochemical evidence indicates that the RIPK3 and caspase-8 axis interacts with inflammasome sensors, forming a large multiprotein complex that triggers PANoptosis during infection with live pathogens and exposure to various PAMPs/DAMPs [11, 13, 14, 35–38, 43]. In the context of IAV infection, ZBP1 senses viral nucleic acids (Z-RNA) and engages with RIPK3 through RHIM domains to recruit caspase-8. This ZBP1-RIPK3-caspase-8 complex initiates three important inflammatory cell death pathways: GSDMD-mediated pyroptosis, caspase-3/caspase-7-mediated apoptosis, and MLKL-mediated necroptosis. Subsequently, RIPK3 and caspase-8 induce the assembly of the NLRP3 inflammasome via ASC and pro-caspase-1 [13, 14]. During HSV1 and *Francisella novicida* infection, AIM2 senses HSV1 dsDNA and recruits ZBP1 and pyrin. ZBP1 then interacts with RIPK3 and RIPK1 through RHIM domains to recruit caspase-8, ASC, and caspase-1 to induce PANoptosis [11]. In contrast, ASC only interacts with caspase-1 and other ASC molecules, leading to the induction of pyroptosis, after treatment with the single inflammasome ligand poly(dA:dT) [11]. When exposed to multiple PAMPs (LPS and Pam3CSK4), NLRP12 forms a multiprotein complex with RIPK3 and caspase-8 to induce PANoptosis [44]. In our current study, we sought to determine whether additional individual members of the larger cell death-inducing complex are necessary for its overall assembly. First, we investigated whether the complex could still form in response to single inflammasome ligands. We observed that ASC interacts with NLRP3, AIM2, NLRC4, Pyrin, caspase-8, and RIPK3 in WT BMDMs after Cocktail treatment. However, ASC can only interact with the specific single inflammasome sensor but not with other inflammasome sensors, caspase-8, and RIPK3 after exposure to the corresponding single inflammasome ligands (Fig. 2A). Second, we examined whether the complex could still assemble in *Nlrp3*$^{-/-}$, *Aim2*$^{-/-}$, *Nlrc4*$^{-/-}$, and *Mefv*$^{-/-}$ BMDMs after Cocktail treatment. Our findings revealed that the loss of NLRP3, AIM2, NLRC4, or Pyrin completely abolished the interaction of caspase-8 with RIPK3 with ASC specks after Cocktail treatment (Fig. 2B). These results suggest that NLRP3, AIM2, NLRC4, and Pyrin interact with ASC specks, which in turn recruit RIPK3 and caspase-8 only in response to treatment with multiple inflammasome ligands (LPS + ATP, poly (dA:dT), flagellin, and TcdB; Cocktail).

Extracellular ASC specks are causative agents that have been observed in patients with asthma [21], chronic obstructive pulmonary disease [22], chronic infantile neurological cutaneous and articular syndrome [23], and Alzheimer's disease [25]. Extracellular ASC specks are internalized by phagocytic cells to induce sterile inflammation by triggering secondary inflammasome activation in the absence of allergens or infectious agents [21–23]. However, the components of extracellular oligomeric inflammasome particles and the contribution of secondary inflammasomes in neighboring phagocytic cells to inflammation and disease remain unclear. Here, we found that activation of the

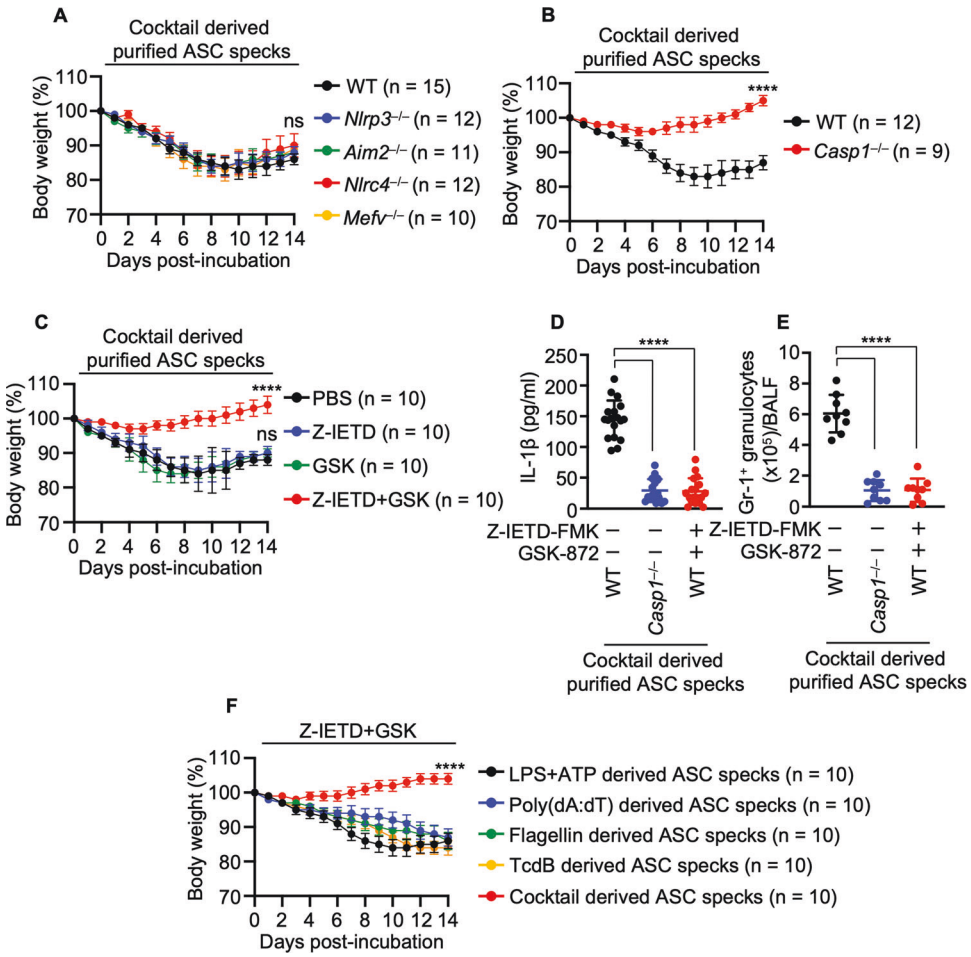

Fig. 7 Extracellular multiple inflammasome particle-driven inflammation depends on caspase-1 or the caspase-8/RIPK3 axis. **A** Body weights of 6- to 8-week-old wild-type (WT), *Nlrp3*$^{-/-}$, *Aim2*$^{-/-}$, *Nlrc4*$^{-/-}$, or *Mefv*$^{-/-}$ mice after the intranasal administration of 5×10^6 particles of purified ASC-Citrine specks after treatment with the combination of LPS + ATP, poly(dA:dT), flagellin, and TcdB (Cocktail). **B** Body weights of 6- to 8-week-old WT or *Casp1*$^{-/-}$ mice after the intranasal administration of 5×10^6 particles of purified ASC-Citrine specks after Cocktail treatment. **C** Body weights of 6- to 8-week-old WT mice intranasally administered PBS, Z-IETD-FMK, GSK-872, or a combination of Z-IETD-FMK and GSK-872 24 h before the intranasal administration of 5×10^6 particles of purified ASC-Citrine specks after Cocktail treatment. **D** The amounts of IL-1β in bronchoalveolar lavage fluid (BALF) from the indicated mice were measured using ELISA 5 days after the intranasal administration of 5×10^6 particles of purified ASC-Citrine specks after Cocktail treatment. Data are mean ± s.e.m. $^{****}P < 0.0001$ (one-way ANOVA with Dunnett's multiple comparisons test; $n = 18$ mice per group). **E** Number of Gr-1+ granulocytes in the BALF from the indicated mice 5 days after the intranasal administration of 5×10^6 particles of purified ASC-Citrine specks after Cocktail treatment. Data are mean ± s.e.m. $^{****}P < 0.0001$ (one-way ANOVA with Dunnett's multiple comparisons test; $n = 9$ mice per group). **F** Body weights of 6- to 8-week-old WT mice intranasally administered a combination of Z-IETD-FMK and GSK-872 24 h before the intranasal administration of 5×10^6 particles of purified ASC-Citrine specks after the indicated treatment. Data are shown as the mean ± SEM (**A**, **B**, **C**, **F**). Data are pooled from three independent experiments (**A**, **B**, **C**, **D**, **E**, **F**)

integrated NLRP3, AIM2, NLRC4, and Pyrin inflammasome by multiple inflammasome ligands led to the release of functional oligomeric inflammasome particles containing NLRP3, AIM2, NLRC4, Pyrin, caspase-8, RIPK3, and ASC, and these particles act as danger signals to amplify inflammation in neighboring macrophages after the internalization of these particles. We also observed new roles for these particles in activating secondary inflammasomes in neighboring phagocytic cells during inflammation and disease. Secondary inflammasome activation by extracellular ASC specks from multiple inflammasome ligand-exposed cells, as identified here, is mediated by caspase-1 and the caspase-8/RIPK3 axis, but it may be similar to PANoptosis, since it is also needed for the induction of inflammatory responses by the caspase-1 and caspase-8/RIPK3. The molecular mechanisms by which caspase-1 and the caspase-8/RIPK3 axis control secondary inflammasome activation require further study. This process may involve distinct host-specific factors, PAMP and DAMP regulatory factors, or transcription factors.

Overall, our findings reveal a critical interaction among NLRP3, AIM2, NLRC4, and Pyrin that drives innate immune responses in response to multiple PAMPs and DAMPs. This regulatory mechanism defines the molecular basis by which exposure to multiple PAMPs or DAMPs can trigger the coordinated activation of multiple inflammasome sensors to form a multiprotein complex and cause inflammatory cell death and inflammatory signaling. Considering the diverse roles of inflammasomes, which range from roles in infection to roles in autoinflammation, development, and cancer, characterizing how they interact with and regulate integrated inflammasome assembly adds to our understanding of the functions of these molecules in innate immunity and inflammatory cell death; additionally, such studies will identify new therapeutic targets for inflammasome-mediated diseases.

MATERIALS AND METHODS

Mice

C57BL/6J (wild type [WT]) (Hyochang Science), *Nlrp3*$^{-/-}$ (Cyagen), *Aim2*$^{-/-}$ (Jackson Laboratory), *Nlrc4*$^{-/-}$ (Cyagen), *Mefv*$^{-/-}$ (Cyagen), *Zbp1*$^{-/-}$ (Cyagen), *Casp1*$^{-/-}$ (Jackson Laboratory), and ASC-Citrine (Jackson Laboratory) mice were purchased from the indicated sources. The mice were group-housed (up to five mice per cage), bred under standard pathogen-free housing conditions in the animal facility of Ulsan National Institute of Science and Technology (UNIST) under a 12-h light/dark cycle (lights on from 7 A.M. to 7 P.M.), and fed standard chow. Both male and female mice were used in this study. Age- and sex-matched 6- to 8-week-old mice were used for the in vivo studies, and 6- to 12-week-old mice were used for the in vitro studies. Cohoused animals were used for in vivo analyses. All the experimental procedures were conducted in accordance with protocols that were approved by the Institutional Animal Care and Utilization Committee of UNIST.

Cell culture

Primary bone marrow-derived macrophages (BMDMs) were cultivated for six days in IMDM (Thermo Fisher Scientific, 12440061) supplemented with 5% FBS (Thermo Fisher Scientific, 16000044), 30% L929-conditioned medium, 1% nonessential amino acids (Thermo Fisher Scientific, 11140-050), and 1% penicillin and streptomycin (Thermo Fisher Scientific, 15070-063). BMDMs were seeded in 12-well plates at a density of 1 million cells per well and incubated overnight before use. L929 cells (ATCC, CCL-1) were purchased and grown in IMDM supplemented with 10% FBS (Thermo Fisher Scientific, 16000044), 1% nonessential amino acids, and 1% penicillin and streptomycin. Primary airway macrophages were isolated from BALF as previously described [21] and grown in RPMI 1640 medium supplemented with 10% FBS and 1% penicillin and streptomycin. WT immortalized bone marrow-derived macrophages (iBMDMs) were a gift from Dr. Tae-Hyuk Kwon (UNIST) and were grown in DMEM (Thermo Fisher Scientific, 11995081) supplemented with 10% FBS and 1% penicillin and streptomycin.

Generation of knockout clonal cells

iBMDM cells were electroporated with 1 μg of a Cas9-encoding plasmid and 1 μg of a gRNA-expressing plasmid via an Amaxa 4D-Nucleofector program DS-136. A total of 4×10^5 cells were used for each electroporation. To generate single cell-derived knockout clones in iBMDM, transfected cells were seeded at a low density of 0.5 cells/well in a 96-well plate. After 10–14 days, each well was examined for the presence of healthy single-cell-derived clones. Single cell-derived clones were detached using trypsin, and genomic DNA was isolated using a DNeasy Blood & Tissue Kit (Qiagen). To confirm target gene knockout in single cell-derived clones, genomic regions containing the Cas9 target site were amplified using KAPA HiFi HotStart PCR polymerase (KK2502). The resulting amplicons were then amplified again using TruSeq HT Dual index-containing primers to generate deep sequencing libraries. The libraries were sequenced using Illumina iSeq with paired-end sequencing systems. Mutation frequencies were calculated using the MAUND program, which is available at https://github.com/ibs-cge/maund.

Virus culture

Human herpes simplex virus 1 (HF strain) (ATCC; VR-260) was purchased and propagated in Vero cells (Korean Cell Line Bank; 10081); the virus titer was measured using the plaque assay in Vero cells. Influenza A virus (A/Puerto Rico/8/34, H1N1 (PR8)) was kindly provided by Dr. Man-Seong Park (Korea University) and propagated in 11-day-old embryonated chicken eggs by allantoic inoculation. The influenza A virus titer was measured using the plaque assay in MDCK cells (gift from Dr. Atsushi Kawaguchi (University of Tsukuba)).

Cell stimulation and infection

For NLRP3 inflammasome activation, cells were primed for 4 h with 500 ng/ml ultrapure LPS from *Escherichia coli* (0111:B4) (InvivoGen, tlrl-3pelps) and then stimulated for 6 h with either 5 μM ATP (Roche, 10127531001) or 1 μM nigericin (InvivoGen, tlrl-nig). For ligand-mediated AIM2 inflammasome activation, 1 ng of poly(dA:dT) (InvivoGen, tlrl-patn) was transfected into cells using DOTAP (Roche, 11202375001) according to the manufacturer's instructions, followed by incubation for 6 h. For NLRC4 inflammasome activation, 10 ng of flagellin (Invivogen, tlrl-epstfla-5) was transfected into cells using DOTAP (Roche, 11202375001) according to the manufacturer's instructions, followed by incubation for 6 h. For Pyrin inflammasome activation, 0.5 μg/ml TcdB (R&D systems, 6246-GT) was transfected into cells using DOTAP (Roche, 11202375001) according to the manufacturer's instructions, followed by incubation for 6 h. For multiple inflammasome activation, cells were primed for 4 h with 500 ng/ml LPS and then transfected with either Cocktail (1 μM Nigericin + 1 ng poly(dA:dT) + 10 ng flagellin + 0.5 μg/ml TcdB) or Cocktail (5 μM ATP + 1 ng poly(dA:dT) + 10 ng flagellin + 0.5 μg/ml TcdB) using DOTAP (Roche, 11202375001) according to the manufacturer's instructions, followed by incubation for 6 h. For HSV1 (12 h; MOI 10) and IAV (12 h; MOI 10) infection, cells were infected in high-glucose DMEM (WElGene, LM001-03). To inhibit caspase-8 and RIPK3, 20 μM Z-IETD-FMK (InvivoGen) and GSK-872 (Millipore) were added to the cells 1 h before treatment. To inhibit caspase-1, 50 μM VX-765 (Chemietek) or 50 μM Ac-YVAD-CMK (InvivoGen) was added to the cells 1 h before treatment.

Real-time cell death analysis

An IncuCyte S3 imaging system (Sartorius) was purchased, and real-time cell death analysis was performed as previously described [11, 20, 40, 45, 46] on an IncuCyte S3 imaging system. BMDMs were seeded in 12-well plates (10^6 cells/well) and stimulated. After incubation, SYTOX Green (Thermo Fisher Scientific, S7020) or propidium iodide (PI; Life Technologies, P3566) was added according to the manufacturer's protocol. Images were acquired every 1 h at 37 °C in 5% CO_2. The resulting images were analyzed using the software supplied with the IncuCyte imager, the number of SYTOX Green-positive BMDM nuclei (Sytox$^+$ BMDM nuclei) or PI-positive BMDM nuclei (PI$^+$ BMDM nuclei) present in each image were counted, and the number of ASC-Citrine-positive BMDMs present in each image were counted.

Cytokine analysis

Cytokine levels were measured using IL-1β ELISA (Invitrogen, BMS6002TEN) or IL-18 ELISA (Invitrogen, BMS618-3TEN) kits according to the manufacturer's instructions.

Immunoblotting analysis

Immunoblotting was performed as previously described [11, 20, 40, 45, 47]. Briefly, for caspase analysis, BMDMs were lysed along with their supernatant using 50 μl caspase lysis buffer (1 × protease inhibitors, 1× phosphatase inhibitors, 10% NP-40, and 25 mM DTT), followed by the addition of 100 μl 4 × SDS loading buffer. For signaling protein analysis, BMDM supernatants were removed at the indicated time points, the cells were washed once with PBS, and the cells were then lysed with RIPA buffer. Proteins were separated by electrophoresis in 8–15% polyacrylamide gels. After the electrophoretic transfer of the proteins to PVDF membranes (Millipore, IPVH00010), nonspecific binding was blocked by incubation with 5% skim milk. The membranes were then incubated with the following primary antibodies: anti-caspase-1 (AdipoGen, AG-20B-0042, 1:1000), anti-caspase-3 (CST, #9662, 1:1000), anti-cleaved caspase-3 (CST, #9661, 1:1000), anti-caspase-7 (CST, #9492, 1:1000), anti-cleaved caspase-7 (CST, #9491, 1:1000), anti-caspase-8 (CST, #4927, 1:1000), anti-cleaved caspase-8 (CST, #8592, 1:1000), anti-pMLKL (CST, #37333, 1:1000), anti-MLKL (Abgent, AP14272b, 1:1000), anti-GSDMD (Abcam, ab209845, 1:1000), anti-GSDME (Abcam, ab215191, 1:1000), anti-NLRP3 (AdipoGen, AG-20B-0014, 1:1000), anti-AIM2 (Abcam, ab119791, 1:1000), anti-NLRC4 (Thermo, PA5-88997, 1:500), anti-pyrin (Abcam, ab195975, 1:1,000), anti-ASC (Millipore, 04-147, 1:1,000), anti-RIPK3 (ProSci, 2283, 1:1,000), anti-ZBP1 (AdipoGen, AG-20B-0010, 1:1000), and anti-β-actin (Proteintech, 66009-1-IG, 1:5000) antibodies. The membranes were then washed and incubated with the appropriate horseradish peroxidase (HRP)-conjugated secondary antibodies (1:5000 dilution; Jackson Immuno Research Laboratories, anti-rabbit [111-035-047], anti-mouse [315-035-047] antibodies) for 1 h. The proteins were visualized using Luminata Forte Western HRP Substrate (Millipore, WBLUF0500), and the membranes were analyzed using Amersham ImageQuant 800 UV.

Immunoprecipitation

Immunoprecipitation was performed as previously described [11, 40, 48]. Briefly, after treatment, cells were lysed in buffer containing 20 mM Tris-HCl (pH 7.4), 100 mM NaCl, 30 mM KCl, and 0.1% NP-40. After centrifugation at 16,000 × *g* for 10 min, the lysates were incubated with IgG control antibody

(CST, 3900S), anti-ASC antibody (AdipoGen; AG-25B-006-C100), or anti-RIPK3 antibody (ProSci, #2283) with protein A/G PLUS-Agarose (Santa Cruz Biotechnology) or protein A Sepharose (GE Healthcare; GE17-5280-01) overnight at 4 °C. After washing with the above buffer, the immunoprecipitated proteins were eluted with 0.1 mM glycine (pH 3.0).

Purification of extracellular ASC specks

Extracellular ASC specks were purified as previously described [21]. Briefly, ASC-Citrine-derived BMDMs were prepared from ASC-Citrine mice, and their supernatants were collected and centrifuged at 150 × *g* for 5 min to remove cell debris 24 h after treatment with a single inflammasome ligand (5 μM ATP, 1 ng poly(dA:dT), 10 ng flagellin, or 0.5 μg/ml TcdB) or the ligand Cocktail (5 μM ATP + 1 ng poly(dA:dT) + 10 ng flagellin + 0.5 μg/ml TcdB). The supernatants were then diluted with an equal volume of buffer A containing 20 mM HEPES-KOH (pH 7.5), 5 mM $MgCl_2$, and 0.5 mM EGTA and centrifuged at 4600 × *g* for 10 min to precipitate the extracellular ASC specks. The extracellular ASC specks were resuspended in buffer A and further purified in a self-generated Percoll gradient at 16,000 × *g* for 60 min at 4 °C. After performing five rounds of washing the extracellular ASC specks with PBS, the number of ASC specks was quantified by counting the Citrine fluorescence-positive ASC specks using the IncuCyte S3 imaging system (Sartorius).

In vivo study of extracellular ASC speck-induced changes in body weight

Age- and sex-matched 6- to 8-week-old mice of the indicated genotypes were anesthetized with 250 mg/kg Avertin and intranasally injected with 5×10^6 particles of purified ASC-Citrine specks in 50 μl PBS. To inhibit caspase-8 and RIPK3, the mice were intraperitoneally administered 1 mg/kg Z-IETD-FMK and/or 2 mmol/kg GSK-872 24 h before intranasal injection with 5×10^6 particles of purified ASC-Citrine specks in 50 μl PBS. The mice were then monitored over a period of 14 days for body weight.

Immunofluorescence staining

Immunofluorescence staining was performed as previously described [11, 21, 41, 48, 49]. Briefly, cells were fixed with 4% PFA for 10 min, permeabilized with PBS containing 0.5% Triton X-100 for 3 min, and incubated in PBS containing 1% skim milk for 1 h. For ASC/CASP8/RIPK3 staining, Alexa Fluor 488 (Thermo Fisher, A20181)-conjugated anti-ASC (Millipore, 04-147), Alexa Fluor 568 (ThermoFisher, A20184)-conjugated anti-RIPK3 (ProSci, 2283), or Alexa Fluor 647 (ThermoFisher, A20186)-conjugated anti-caspase-8 (Enzo, 1G12) antibodies were prepared according to the manufacturer's instructions, and coverslips were incubated with the indicated antibodies (1:100) for 1 h. For ASC/NLRP3/AIM2/NLRC4/Pyrin staining, Alexa Fluor 488 (ThermoFisher, A20181)-conjugated anti-ASC (Millipore, 04-147), Alexa Fluor 532 (ThermoFisher, A20182)-conjugated anti-NLRP3 (AdipoGen, AG-20B-0014), Alexa Fluor 568 (ThermoFisher, A20184)-conjugated anti-AIM2 (Abcam, ab119791), Alexa Fluor 647 (ThermoFisher, A20186)-conjugated anti-NLRC4 (Thermo, PA5-88997), Alexa Fluor 680 (ThermoFisher, A20188)-conjugated anti-pyrin (Abcam, ab195975) antibodies were prepared according to the manufacturer's instructions, and coverslips were incubated with the indicated antibodies (1:100) for 1 h. For ASC/tubulin staining, the coverslips were incubated with anti-ASC (Millipore, 04-147) and anti-tubulin (CST, 2144) antibodies. The secondary antibodies that were used were Alexa Fluor 488-conjugated anti-mouse IgG (Life Technologies, A21202; 1:200) and Alexa Fluor 568-conjugated anti-rabbit IgG (Life Technologies, A10042; 1:200). To confirm ASC-Citrine speck engulfment, cells were fixed with 3% PFA and permeabilized with PBS containing 0.5% Triton X-100; the coverslips were then incubated with Alexa Fluor 568-conjugated phalloidin for 1 h. The cells were counterstained with DAPI mounting medium (P36931; Invitrogen). Images were acquired by confocal laser scanning microscopy (LSM980; Carl Zeiss) using a 63× Apochromat objective.

In vivo leukocyte migration analysis

Cells were collected from BALF, resuspended in buffer containing 154 mM NH_4Cl, 10 mM $KHCO_3$, and 0.1 mM EDTA, and incubated for 5 min to lyse the red blood cells. After washing with PBS containing 2% FBS, the cells were then stained with anti-Gr-1 (BioLegend; 108412) antibody for 30 min on ice. The stained cells were analyzed using the IncuCyte S3 imaging system (Sartorius).

Statistical analysis

GraphPad Prism 8.0 software was used for data analysis. The data are presented as the mean ± SEM. Statistical significance was determined using a *t* test (two-tailed) or one-way ANOVA with multiple comparisons for multiple groups. *P* values less than 0.05 were considered statistically significant and are indicated as $^*P < 0.05$, $^{**}P < 0.01$, $^{***}P < 0.001$, and $^{****}P < 0.0001$.

DATA AND MATERIALS AVAILABILITY

All the data are available in the main text or the supplementary materials.

REFERENCES

1. Man SM, Karki R, Kanneganti TD. Molecular mechanisms and functions of pyroptosis, inflammatory caspases and inflammasomes in infectious diseases. Immunol Rev. 2017;277:61–75.
2. Boyden ED, Dietrich WF. Nalp1b controls mouse macrophage susceptibility to anthrax lethal toxin. Nat Genet. 2006;38:240–4.
3. Sandstrom A, Mitchell PS, Goers L, Mu EW, Lesser CF, Vance RE. Functional degradation: a mechanism of NLRP1 inflammasome activation by diverse pathogen enzymes. Science. 2019;364:eaau1330.
4. Chui AJ, Okondo MC, Rao SD, Gai K, Griswold AR, Johnson DC, et al. N-terminal degradation activates the NLRP1B inflammasome. Science. 2019;364:82–5.
5. Robinson KS, Teo DET, Tan KS, Toh GA, Ong HH, Lim CK, et al. Enteroviral 3C protease activates the human NLRP1 inflammasome in airway epithelia. Science. 2020;370:eaay2002.
6. Bauernfried S, Scherr MJ, Pichlmair A, Duderstadt KE, Hornung V. Human NLRP1 is a sensor for double-stranded RNA. Science. 2021;371:eabd0811.
7. Karki R, Man SM, Malireddi RKS, Gurung P, Vogel P, Lamkanfi M, et al. Concerted activation of the AIM2 and NLRP3 inflammasomes orchestrates host protection against Aspergillus infection. Cell Host Microbe. 2015;17:357–68.
8. Broz P, Newton K, Lamkanfi M, Mariathasan S, Dixit VM, Monack DM. Redundant roles for inflammasome receptors NLRP3 and NLRC4 in host defense against Salmonella. J Exp Med. 2010;207:1745–55.
9. Man SM, Hopkins LJ, Nugent E, Cox S, Glück IM, Tourlomousis P, et al. Inflammasome activation causes dual recruitment of NLRC4 and NLRP3 to the same macromolecular complex. Proc Natl Acad Sci USA. 2014;111:7403–8.
10. Kalantari P, DeOliveira RB, Chan J, Corbett Y, Rathinam V, Stutz A, et al. Dual engagement of the NLRP3 and AIM2 inflammasomes by plasmodium-derived hemozoin and DNA during malaria. Cell Rep. 2014;6:196–210.
11. Lee S, Karki R, Wang Y, Nguyen LN, Kalathur RC, Kanneganti TD. AIM2 forms a complex with pyrin and ZBP1 to drive PANoptosis and host defence. Nature. 2021;597:415–9.
12. Christgen S, Zheng M, Kesavardhana S, Karki R, Malireddi RKS, Banoth B, et al. Identification of the PANoptosome: a molecular platform triggering pyroptosis, apoptosis, and necroptosis (PANoptosis). Front Cell Infect Microbiol. 2020;10:237.
13. Kuriakose T, Man SM, Malireddi RK, Karki R, Kesavardhana S, Place DE, et al. ZBP1/DAI is an innate sensor of influenza virus triggering the NLRP3 inflammasome and programmed cell death pathways. Sci Immunol. 2016;1:aag2045-aag2045.
14. Zheng M, Karki R, Vogel P, Kanneganti TD. Caspase-6 is a key regulator of innate immunity, inflammasome activation, and host defense. Cell. 2020;181:674–687.e13.
15. Zheng M, Williams EP, Malireddi RKS, Karki R, Banoth B, Burton A, et al. Impaired NLRP3 inflammasome activation/pyroptosis leads to robust inflammatory cell death via caspase-8/RIPK3 during coronavirus infection. J Biol Chem. 2020;295:14040–52.
16. Fritsch M, Günther SD, Schwarzer R, Albert MC, Schorn F, Werthenbach JP, et al. Caspase-8 is the molecular switch for apoptosis, necroptosis and pyroptosis. Nature. 2019;575:683–7.
17. Newton K, Wickliffe KE, Maltzman A, Dugger DL, Reja R, Zhang Y, et al. Activity of caspase-8 determines plasticity between cell death pathways. Nature. 2019;575:679–82.
18. Schwarzer R, Jiao H, Wachsmuth L, Tresch A, Pasparakis M. FADD and caspase-8 regulate gut homeostasis and inflammation by controlling MLKL- and GSDMD-mediated death of intestinal epithelial cells. Immunity. 2020;52:978–993.e6.
19. Doerflinger M, Deng Y, Whitney P, Salvamoser R, Engel S, Kueh AJ, et al. Flexible usage and interconnectivity of diverse cell death pathways protect against intracellular infection. Immunity. 2020;53:533–547.e7.
20. Karki R, Lee S, Mall R, Pandian N, Wang Y, Sharma BR, et al. ZBP1-dependent inflammatory cell death, PANoptosis, and cytokine storm disrupt IFN therapeutic efficacy during coronavirus infection. Sci Immunol. 2022:eabo6294.

21. Lee S, Ishitsuka A, Kuroki T, Lin YH, Shibuya A, Hongu T, et al. Arf6 exacerbates allergic asthma through cell-to-cell transmission of ASC inflammasomes. JCI Insight. 2021;6.
22. Franklin BS, Bossaller L, De Nardo D, Ratter JM, Stutz A, Engels G, et al. The adaptor ASC has extracellular and 'prionoid' activities that propagate inflammation. Nat Immunol. 2014;15:727–37.
23. Baroja-Mazo A, Martin-Sanchez F, Gomez AI, Martinez CM, Amores-Iniesta J, Compan V, et al. The NLRP3 inflammasome is released as a particulate danger signal that amplifies the inflammatory response. Nat Immunol. 2014;15:738–48.
24. Sagoo P, Garcia Z, Breart B, Lemaitre F, Michonneau D, Albert ML, et al. In vivo imaging of inflammasome activation reveals a subcapsular macrophage burst response that mobilizes innate and adaptive immunity. Nat Med. 2016;22:64–71.
25. Venegas C, Kumar S, Franklin BS, Dierkes T, Brinkschulte R, Tejera D, et al. Microglia-derived ASC specks cross-seed amyloid-beta in Alzheimer's disease. Nature. 2017;552:355–61.
26. Lee S, Cho HJ, Ryu JH. Innate immunity and cell death in Alzheimer's disease. ASN Neuro. 2021;13:17590914211051908.
27. Kanneganti TD, Ozören N, Body-Malapel M, Amer A, Park JH, Franchi L, et al. Bacterial RNA and small antiviral compounds activate caspase-1 through cryopyrin/Nalp3. Nature. 2006;440:233–6.
28. Fernandes-Alnemri T, Yu JW, Datta P, Wu J, Alnemri ES. AIM2 activates the inflammasome and cell death in response to cytoplasmic DNA. Nature. 2009;458:509–13.
29. Hornung V, Ablasser A, Charrel-Dennis M, Bauernfeind F, Horvath G, Caffrey DR, et al. AIM2 recognizes cytosolic dsDNA and forms a caspase-1-activating inflammasome with ASC. Nature. 2009;458:514–8.
30. Zhao Y, Yang J, Shi J, Gong YN, Lu Q, Xu H, et al. The NLRC4 inflammasome receptors for bacterial flagellin and type III secretion apparatus. Nature. 2011;477:596–600.
31. Xu H, Yang J, Gao W, Li L, Li P, Zhang L, et al. Innate immune sensing of bacterial modifications of Rho GTPases by the Pyrin inflammasome. Nature. 2014;513:237–41.
32. Vladimer GI, Weng D, Paquette SW, Vanaja SK, Rathinam VA, Aune MH, et al. The NLRP12 inflammasome recognizes Yersinia pestis. Immunity. 2012;37:96–107.
33. Lee S, Channappanavar R, Kanneganti TD. Coronaviruses: innate immunity, inflammasome activation, inflammatory cell death, and cytokines. Trends Immunol. 2020;41:1083–99.
34. Place DE, Lee S, Kanneganti TD. PANoptosis in microbial infection. Curr Opin Microbiol. 2021;59:42–9.
35. Karki R, Sharma BR, Tuladhar S, Williams EP, Zalduondo L, Samir P, et al. Synergism of TNF-α and IFN-γ triggers inflammatory cell death, tissue damage, and mortality in SARS-CoV-2 infection and cytokine shock syndromes. Cell. 2021;184:149–168.e17.
36. Malireddi RKS, Gurung P, Mavuluri J, Dasari TK, Klco JM, Chi H, et al. TAK1 restricts spontaneous NLRP3 activation and cell death to control myeloid proliferation. J Exp Med. 2018;215:1023–34.
37. Lamkanfi M, Kanneganti TD, Van Damme P, Vanden Berghe T, Vanoverberghe I, Vandekerckhove J, et al. Targeted peptidecentric proteomics reveals caspase-7 as a substrate of the caspase-1 inflammasomes. Mol Cell Proteom. 2008;7:2350–63.
38. Gurung P, Anand PK, Malireddi RK, Vande Walle L, Van Opdenbosch N, Dillon CP, et al. FADD and caspase-8 mediate priming and activation of the canonical and noncanonical Nlrp3 inflammasomes. J Immunol. 2014;192:1835–46.
39. Malireddi RKS, Gurung P, Kesavardhana S, Samir P, Burton A, Mummareddy H, et al. Innate immune priming in the absence of TAK1 drives RIPK1 kinase activity-independent pyroptosis, apoptosis, necroptosis, and inflammatory disease. J Exp Med. 2020;217.
40. Karki R, Sundaram B, Sharma BR, Lee S, Malireddi RKS, Nguyen LN, et al. ADAR1 restricts ZBP1-mediated immune response and PANoptosis to promote tumorigenesis. Cell Rep. 2021;37:109858.
41. Wang Y, Pandian N, Han JH, Sundaram B, Lee S, Karki R, et al. Single cell analysis of PANoptosome cell death complexes through an expansion microscopy method. Cell Mol Life Sci. 2022;79:531.
42. Tzeng TC, Schattgen S, Monks B, Wang D, Cerny A, Latz E, et al. A fluorescent reporter mouse for inflammasome assembly demonstrates an important role for cell-bound and free ASC specks during in vivo infection. Cell Rep. 2016;16:571–82.
43. Oh S, Lee S. Recent advances in ZBP1-derived PANoptosis against viral infections. Front Immunol. 2023;14:1148727.
44. Sundaram B, Pandian N, Mall R, Wang Y, Sarkar R, Kim HJ, et al. NLRP12-PANoptosome activates PANoptosis and pathology in response to heme and PAMPs. Cell. 2023;186:2783–801.e20.
45. Wang Y, Karki R, Zheng M, Kancharana B, Lee S, Kesavardhana S, et al. Cutting edge: Caspase-8 is a linchpin in caspase-3 and gasdermin D activation to control cell death, cytokine release, and host defense during influenza A virus infection. J Immunol. 2021;207:2411–6.
46. Wang Y, Karki R, Mall R, Sharma BR, Kalathur RC, Lee S, et al. Molecular mechanism of RIPK1 and caspase-8 in homeostatic type I interferon production and regulation. Cell Rep. 2022;41:111434.
47. Tweedell RE, Malireddi RKS, Kanneganti TD. A comprehensive guide to studying inflammasome activation and cell death. Nat Protoc. 2020;15:3284–333.
48. Lee S, Ishitsuka A, Noguchi M, Hirohama M, Fujiyasu Y, Petric PP, et al. Influenza restriction factor MxA functions as inflammasome sensor in the respiratory epithelium. Sci Immunol. 2019;4:eaau4643.
49. Lee S, Hirohama M, Noguchi M, Nagata K, Kawaguchi A. Influenza A virus infection triggers pyroptosis and apoptosis of respiratory epithelial cells through the type I interferon signaling pathway in a mutually exclusive manner. J Virol. 2018;92:10-1128.

ACKNOWLEDGEMENTS

We thank Rajendra Karki (Seoul National University) and the members of the Lee lab (Viral Immunology Lab) for their helpful comments and suggestions. We thank Man-Seong Park (Korea University) for the gift of the influenza A virus (PR8) and Tae-Hyuk Kwon (UNIST) for the gift of the iBMDMs. We also thank Atsushi Kawaguchi (University of Tsukuba) for the gift of the MDCK cells.

AUTHOR CONTRIBUTIONS

SL conceptualized the study; SO, JL, and SL designed the methodology; SO, JL, JO, GY, HK, DK, and SL performed the experiments; SO, JL, and SL conducted the analysis; SO and SL wrote the manuscript; SL acquired the funding and provided overall supervision.

FUNDING

This research was supported by the National Research Foundation of Korea (NRF) grant that was funded by the Korean government (MSIT) (2022R1C1C1007544 to SL), by a grant from the Korea Health Technology R&D Project through the Korea Health Industry Development Institute (KHIDI) that was funded by the Ministry of Health & Welfare, Republic of Korea (HV22C015600 to SL), by grants from the National Institute of Health, Republic of Korea (2022-NI-072-00 to SL), by the Institute for Basic Science (IBS), Republic of Korea (IBS-R801-D9-A09 to SL), by a research fund from Ulsan National Institute of Science & Technology (UNIST) (1.220112.01, 1.220107.01 to SL), by a grant from Yuhan Corporation (SL), by the National Research Foundation of Korea (NRF) and the Center for Women In Science, Engineering and Technology (WISET) grant that was funded by the Ministry of Science and ICT (MSIT) under the Program for Returners into R&D (to JL).

COMPETING INTERESTS

The authors declare no competing interests.

ADDITIONAL INFORMATION

Supplementary information The online version contains supplementary material available at https://doi.org/10.1038/s41423-023-01107-9.

Correspondence and requests for materials should be addressed to SangJoon Lee.

Reprints and permission information is available at http://www.nature.com/reprints